Applying a Modified Two-Fluid Model to Numerical Simulation of Two-Phase Flow in the Membrane Chlor-Alkali Cells

Abbasi, Farshad*[+]; Rahimzadeh, Hasan
Department of Mechanical Engineering, Amirkabir University of Technology, Tehran, I.R. IRAN

ABSTRACT: *In this study, gas evolution in a vertical electrochemical cell is investigated numerically with a modified two-fluid model. The mathematical model involves solution of separate transport equation for the gas and liquid phases with an allowance to inter-phase transfer of mass and momentum. The governing equations are discreted via the finite volume technique and then are solved by the SIMPLE algorithm in both the natural and forced convection states. In order to increase the accuracy of calculations, the power-law scheme is employed to approximate the convection-diffusion terms. Void fraction distribution of chlorine gas and velocity of both the gas and liquid phases are calculated. Also the effect of current density, electrolyte flow rate and space between the electrodes on the gas release are investigated. To verify this model, numerical simulations of a bubble-driven flow caused by the bottom injection of gas into a liquid bath is conducted. Comparisons between the predictions and the literature numerical datas illustrate that the predicted results satisfactorily agree with data available in the literature for both the liquid and gas phases.*

KEY WORDS: *Membrane cells, Two-phase flow, Two-fluid model, Chlor-alkali, Numerical simulation.*

INTRODUCTION

Electrochemical reaction is largely employed in various industrial processes such as hydrogen production, chlorineate process, electroplating, metal purification, etc. Most of these processes often take place with gas evolution on the electrodes. The presence of gas phase in the liquid phase makes the problem a two-phase flow being the knowledge available from heat transfer and fluid mechanics studies. Bubbles significantly affect mass transfer, flow field, the conductivity of bulk electrolyte and macroscopic current density distribution which is crucial in determination of the reaction r ate. The major aim of this study is to investigate chlorine gas release in an electrolysis process from two-phase flow point of view and to investigate the effect of gas release on the electrolysis process. Gas bubbles form and grow at the electrode surface as a result of the electrochemical reaction and leave the surface when buoyancy and shear forces are applied on a bubble, exceed the interfacial

* To whom correspondence should be addressed.
+ E-mail: farshadmit@yahoo.com
1021-9986/08/3/51 11/$/3.10

tension forces. Except the forced electrolyte flow, main driving mechanism for flow in such systems are buoyancy due to density difference between liquid and gas phases and concentration gradient across the cell. The presence of bubbles is known to cause a local turbulence or chaotic flow which is very efficient in mixing and local distribution of the species.

There have been numerous experimental and theoretical studies on the determination of void fraction, the species transport, and the flow regimes occurring in electrochemical cells. *Vogt* [1] performed a variety of experiments to observe the gas release behavior on an electrolysis cell and showed that at the low current densities, evolved gas leaved the surface mainly by molecular diffusion. At higher current densities, gas bubbles were nucleated at several locations on the electrode and grown with dissolved gas in the electrolyte. It was also shown that only a small portion of gas evolved on the electrode, most of the contribution came from the supersaturated electrolyte adjacent to electrode surface. *Reigel et al*. [2] identified two flow regimes in an electrolyzer cell depending on the current density. At low current densities, gas evolution became small and two-phase flow region confined in a very small region adjacent to the electrode, however, at higher current densities, a back flow leading occurred by the increase of electrolyte resistance.

In a range of current density *Fukunaka et al.* [3] found that the mass transfer coefficient increased at higher current densities. This trend was attributed to transition to turbulence at higher current densities. *Boissanneau* and *Byrne* [4] investigated velocity field in an electrochemical cell with vertical electrodes for chlorineine production. Advanced measurement systems such as Laser Doppler Anemometry and particle image velocitymetry were employed to determine flow field. They showed that even though the flow was laminar in terms of relevant Reynolds number range considered, bubbles caused local turbulence by causing velocity fluctuations due to the interactions with continuous phase. Therefore, both laminar and turbulent regimes exist in the system.

The bubbles growth and accumulation on the electrodes significantly affect the conductivity of the electrolyte mainly reducing the active area. *Hine* and *Murakami* [5] measured current density under the forced and natural convection states. They found that the current density significantly decreased along the electrode in a bottom-up direction due to the bubble enrichment.

In a recent experiment *Nagai et al.* [6] investigated several process parameters such as temperature, height of the electrodes and space between the electrodes on the performance of the cell. They found that smaller space between the electrodes reduced the efficiency of the system. *Byrne et al.* [7] developed a mathematical model considering a simple Poiselle flow, while the effects of bubbles on the velocity profile were not accounted for. Using a comprehensive model, *Ozil et al.* [8] estimated the voltage and the velocity distributions across a chlorineate cell and evaluated the natural convection in the system. Two-phase pressure drop was calculated using correlation developed by *Lockart* and *Martinelli* [9]. *Heal et al.* [10] employed a mathematical model which combined hydrodynamics diffusion layer and a bubble diffusion layer identified by *Janssen* and *Hoogland* [11]. *Boxall* and *Kelsall* [12] divided diffusion layer into two parts. The first domain involved the hydrolysis reaction existing in equilibrium, while the second layer assumes this reaction as the first order and irreversible.

Recently, *Dahlkild* [13] applied a mixture of two-phase flow model for electrolysis process and modified the model by applying a boundary layer analysis. The numerical results of *Dahlkild* showed that the non-uniform bubble distributions along the electrodes would result in a non-uniform current density distribution.

The single fluid mixture model considers gas-liquid mixture as a single fluid with a variable density. The main drawback of this method is the calculation of gas phase distribution. This distribution may be either obtained from experimental data or by solving a separate transport equation [14]. The mixture model is also not adequate to predict the flow behavior of each phase. The two-phase flow models have no such limitations. In a recent study, *Mat et al*. [15] developed a two-fluid mathematical model for hydrogen production in a forced flow electrochemical system and found that the model successfully captures the main characteristics of the electrolysis process.

Therefore, the target of this study is mainly to adopt the two-phase model developed by *Mat et al.* [15] and *Jinsong et al.* [16] and applying it to a chlorine-evolving membrane cell and to study the effects of various parameters on the system performance in a laminar regime. To verify this model, numerical simulations of a bubble-driven flow caused by the bottom injection of

gas into a liquid bath is conducted. Comparisons between the predictions and the literature numerical data of *Jinsong et al.* [16] illustrate that the present model is capable of capturing a reasonable agreement with numerical results for both the liquid and gas phases.

PHYSICAL PROBLEM

The schematic sketch of problem considered is given in Fig. 1. The system consists of two electrodes, named cathode and anode located on the right and the left walls of the membrane respectively, and an electrolyte being a dilute solution of NaCl in the water. The hydrogen gas evolved at the cathode and chlorine gas at the anode after passing a current between the two electrodes.

NaCl dissociates into Na^+ and Cl^- ions and hydrogen gas evolves at the cathode while chlorine gas forms at the anode according to the following electro-chemical reactions:

At the cathode

$$2H_2O + 2e^- \rightarrow 2OH^- + H_2 \qquad (1)$$
$$2Na^+ + 2OH^- \rightarrow 2NaOH$$

At the anode

$$2NaCl \rightarrow 2Na^+ + 2Cl^- \qquad (2)$$
$$2Cl^- \rightarrow Cl_2 + 2e^-$$

Since chlorine evolution is the primary purpose of the electrolysis, only the region between the anode and membrane is considered in this study. Configuration and dimensions of the system are considered as the mirror of the experimental study of *Jean St-Pierre et al.* [17].

GOVERNING EQUATIONS

In order to represent the flow behavior and heat transfer in the system, a two-phase mixture of the liquid and gas was considered. The phases were assumed to share some spaces in proportion to their existence probabilities in such a way that their sum of the volume fractions would reach to a unity in the flow field [14,15,18,19]. This assumption can be expressed mathematically as:

$$\alpha_g + \alpha_l = \left(\frac{V_g}{V} + \frac{V_l}{V}\right) = 1 \qquad (3)$$

where α_l , α_g are the volume fractions of the liquid and the gas, respectively. The zone-averaged quantities are obtained through the solution of separate transport equations for each phase. Within this framework, the governing equations for the steady-state; two-phase flow system can be expressed in Cartesian coordinates as follows [14,15,18,19]:

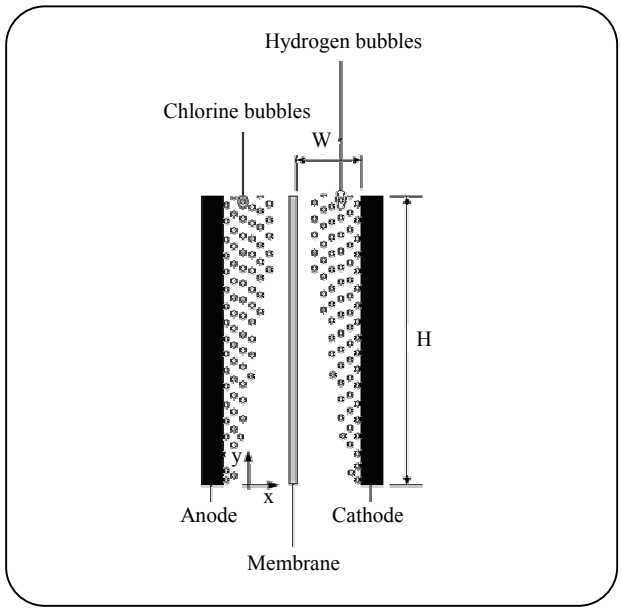

Fig. 1: Schematic sketch of the system considered.

Mass Conservation

$$\frac{\partial}{\partial t}(\alpha_i \rho_i) + \frac{\partial}{\partial x}(\rho_i \alpha_i u_i) + \frac{\partial}{\partial y}(\rho_i \alpha_i v_i) = M_{i-int} \qquad (4)$$

where subscript, i represents the phases and takes the values of l and g in this problem. Subscripts l and g refer to the liquid and the gas phases, respectively, in this and subsequent formulations. The term on the right of the equation represents mass diffusion between the two phases at the electrolyte-gas interface. The mass diffusion at the gas–liquid interface is calculated as [14,15,18,19]:

$$M_{i-int} = \frac{\partial}{\partial x}(\rho_i D_i \frac{\partial \alpha_i}{\partial x}) + \frac{\partial}{\partial y}(\rho_i D_i \frac{\partial \alpha_i}{\partial y}), \qquad (5)$$

where D_i represents diffusion coefficient of phase i and may be expressed as [15,18,19]:

$$D_i = \mu_{eff,i}, \qquad (6)$$

where $\mu_{eff,i}$ is the effective viscosity of phase i and expressed as [14]:

$$\mu_{eff,i(laminar)} = \mu_i \quad (7)$$

$$\mu_{eff,i(turbulent)} = \mu_i + \mu_t$$

where μ_i is the thermodynamic viscosity of phase i and μ_t is the effect of turbulent. Diffusion may affect mass transfer in both the continuous and dispersed phases. For the continuous phase, the convective mass flux is much larger than the diffusive flux, so the diffusion term is negligible [14].

X-momentum

$$\frac{\partial}{\partial t}(\rho_i\alpha_i u_i) + \frac{\partial}{\partial x}(\rho_i\alpha_i u_i^2) + \frac{\partial}{\partial y}(\rho_i\alpha_i u_i v_i) = \quad (8)$$

$$-\frac{\partial}{\partial x}(p\alpha_i) + F_r(u_j - u_i) + \frac{\partial}{\partial x}(\alpha_i\mu_{eff_i}\frac{\partial u_i}{\partial x}) + \frac{\partial}{\partial y}(\alpha_i\mu_{eff_i}\frac{\partial u_i}{\partial y})$$

Y-momentum

$$\frac{\partial}{\partial t}(\rho_i\alpha_i v_i) + \frac{\partial}{\partial x}(\rho_i\alpha_i u_i v_i) + \frac{\partial}{\partial y}(\rho_i\alpha_i v_i^2) = \quad (9)$$

$$-\frac{\partial}{\partial y}(p\alpha_i) + F_r(v_j - v_i) + \frac{\partial}{\partial x}(\alpha_i\mu_{eff_i}\frac{\partial v_i}{\partial x}) + \frac{\partial}{\partial y}(\alpha_i\mu_{eff_i}\frac{\partial v_i}{\partial y}) + F_b$$

$F_b=\rho g$ is the buoyancy force where g being the gravity vector. F_r in both momentum equations is in interface friction term and represents momentum exchange between the phases per unit volume and can be expressed as [20]:

$$F_r = \frac{3}{4}C_d\alpha_g\alpha_l\frac{\mu_l}{d_b^2}Re_b \quad (10)$$

where C_d is the drag coefficient. Assuming that bubbles have a spherical shape with a characteristic diameter of d_b, the drag coefficient is given by [14]:

$$C_d = \begin{cases} \frac{24}{Re_b}, & \text{laminar} \\ \frac{24}{Re_b}(1+0.15Re_b^{0.687}), & \text{turbulent} \end{cases} \quad (11)$$

where Re_b is the Reynolds number based on the gas bubble diameter [14]:

$$Re_b = \frac{\rho_l|U_l - U_g|d_b}{\mu_l} \quad (12)$$

Where $|U_l-U_g|$ is the slip velocity vector between the two phases.

BOUNDARY CONDITIONS

A no-slip condition is applied on the electrode and the membrane surfaces (i.e. vertical walls) for the liquid phase and tangential velocity for the gas phase expressed mathematically as:

$$u_l = v_l = v_g = 0 \quad (13)$$

The normal component of gas phase velocity can be calculated using Faraday's law. Assuming all chlorine produced as a result of electrochemical reaction transform into the gaseous phase, the normal velocity component at the anode (chlorine producing electrode) can be expressed as [15,18,19]:

$$u_g = \frac{1}{2}\frac{RT}{P_{cl_2}}\frac{i(y)}{F} \quad (14)$$

where T, R, P, F are temperature (assumed to be constant in this study), universal gas constant, pressure of gaseous phase and Faraday constant, respectively. The multiplication of normal velocity with electrode surface area gives volumetric production of chlorine gas. The factor 1/2 represents the fact that two electrons must be transferred for the production of each chlorine molecule. $i(y)$ is the current density at the electrode surface and is calculated as [15,18,19,21]:

$$i(y) = -i_0(1-\alpha_g)\exp(-\frac{F}{2RT}\eta) \quad (15)$$

where i_0 is the exchange current density, $(1-\alpha_g)$ represents reduction of the active electrode area due to the bubbles on the electrode. η is the cathodic over potential and expressed as:

$$\eta = -\phi \quad (16)$$

where ϕ represents the electric potential.

Also the no-permeability condition is applied on the electrode and the membrane surfaces for the liquid and gas phases and can be expressed mathematically as:

$$\frac{\partial\alpha_g}{\partial x} = \frac{\partial\alpha_l}{\partial x} = 0 \quad (17)$$

NUMERICAL METHOD

The governing equations for the two-fluid model are solved using the appropriate algebraic equations derived by integrating over the meshed control volume. For this

Table 1: Physical configuration for the laminar bubble-driven flow (Durst et al [22]).

Diameter of container (R)	0.1 (m)	Bubble diameter (d_b)	$6*10^{-3}$ (m)
Liquid depth (H)	0.098 (m)	Gas injection rate (Q)	$2.6*10^{-7}$ (m^3/s)
Density of liquid (ρ_l)	960.3 (kg/m^3)	Gas density (ρ_g)	1.29 (kg/m^3)
Viscosity of liquid (μ_l)	0.6712 ($N\ s/m^2$)	Viscosity of gas (μ_g)	$1.64*10^{-5}$ ($N\ s/m^2$)

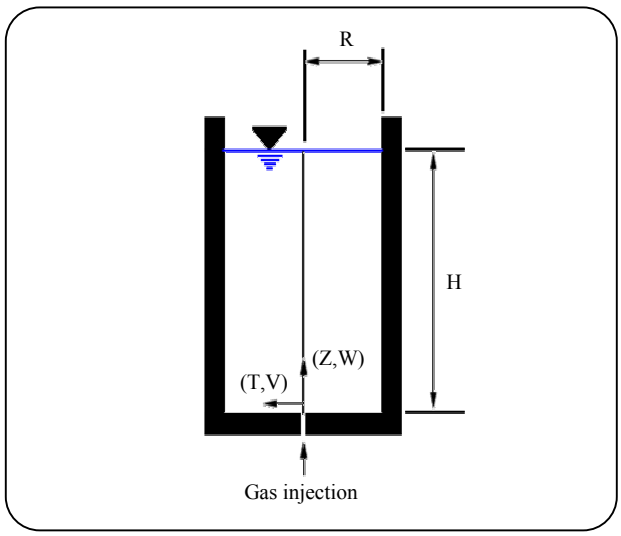

Fig. 2: Schematic diagram of a bubble-driven liquid flow.

purpose, the computational domain is overlaid with an orthogonal uniform grid with the nodal points of velocity variables for each phase being staggered with respect to those of pressure, located at the regular grid nodes. The governing equations are integrated over a control volume by which flow domain is divided and the following algebraic equation is obtained:

$$a_P\phi_P = a_E\phi_E + a_W\phi_W + a_N\phi_N + a_S\phi_S + b \qquad (18)$$

In which a's represent convection and diffusion coefficient and subscripts W, E, S, N represent west, east, south and north of node P and also b represents the volumetric fluid interaction coefficient. In addition, a power-low scheme is employed to approximate the convection and diffusion terms. The whole set of equations is solved by incorporating the SIMPLE algorithm of *Patankar* and *Spalding* (1972). Because of the nonlinearity of the governing equations and the coupling of variables, iterative numerical procedures are conducted until the convergence is reached. The solution is assumed to converge when the term b in the pressure correction equation has fallen below a specified level. In this study, it is assumed that the convergence is reached when $b \leq 0.001$. Furthermore, grid sensitivity is examined to ensure sufficient spatial resolution. The results reported are based on the mesh of 45×200 uniform grids.

CASE STUDY

LAMINAR BUBBLE DRIVEN-LIQUID FLOW

In order to verify the predicted results of this model, numerical investigation of bubbly flow caused by the bottom injection of gas into a cylinder is investigated. The cylinder is filled with castor oil of which the kinematics viscosity is sufficiently large to ensure liquid flow to be in the laminar regime. The schematic sketch of the problem considered is given in Fig. 2. In such a system, gas is injected into a liquid bath (with a depth of H and a diameter of R) from an orifice located at the bottom wall of a cylindrical vessel at a steady state flow rate, as shown in Fig. 2. In this figure, r and z represents the radial and axial coordinates, respectively. v and w stand for the velocity components in radial and axial directions, respectively. The actual dimensions of the liquid container and gas injection rates are specified according to the available experimental data's of *Durst et al.* [22]. The configuration parameters for the simulation are listed in table 1.

There are extensive studies available in the literature investigating bubbly flow hydrodynamics in the cylindrical coordinate. *Durst et al.* [22] performed experimental studies on bubble-driven laminar flows by investigating liquid circulation and bubble's street with Laser-Doppler system. In their experiments, the flow was established in a glass cylinder of 100 mm i.d. with bubbles generated at a 0.5 mm dia. nozzle located at the centre of the bottom wall of container. The cylinder was filled with castor oil of which the kinematics viscosity was sufficiently large to ensure liquid flow to be in the laminar regime. Air was passed through a well-controlled pressure regulator and the resulting bubbles

left the nozzles at a steady rate of one for every 0.55 s with diameter d_b of about 5.0-6.5 mm. Two depths of liquid (H=0.098 m and H=0.278 m) were investigated to determine the profiles of the liquid and the bubble velocities. *Durst et al.* [23] also conducted numerical simulations on the bubble-driven flows at which both the single-phase model and the two-fluid model were used. In the two-fluid model, momentum equations for the liquid phase were derived from the Navier-Stokes equation, while equations for the gas-phase were simplified by neglecting the viscous forces.

Celik and *Wang* [24] used a modified drift-flux model to simulate the problem with the same operating parameters as the experiments by *Durst et al.* [23]. It was reported that the liquid-phase circulation pattern is not sensitive to the actual shape of the void fraction profiles. Detailed predictions on liquid phase are given in their studies, while the corresponding ones for the gas phase are not complete.

Johansen et al. [25] studied the fluid dynamics in bubble-stirred ladles by employing a Laser-Doppler system to measure the axial and radial mean velocities of liquid phase. Air was supplied through a porous plug placed in the bottom wall of a cylindrical Perspex-water model of a ladle. However, no measurement on the gas phase was conducted. *Johansen* and *Boysan* [26] proposed a mathematical model to describe the fluid flow in the bubble-stirred ladle at which Eulerian and Lagrangian methods were used to analyse the liquid and the gas phases, respectively. A limited number of comparisons were conducted between simulations and experimental results of the liquid phase, but no information on the gas phase was reported.

Castillejos and *Brimacombe* [27] studied the plume formation and liquid circulation induced by gas injection at the bottom of cylindrical water containers. They developed an electro-resistivity probe to measure the detailed bubble characteristics such as gas volume fraction, bubble velocity and size. In addition, the axial and radial components of the liquid velocity surrounding the plume were measured by means of a Laser-Doppler system. *Jinsong et al.* [16] applied the two-fluid model to numerical investigation of bubbly flow in a cylinder with bottom gas injection. In their study the hybrid scheme employed to approximate the convection and diffusion terms. In addition, they used the same operating parameters as the experiments by *Durst et al.* [22]. By Comparisons between the predicted and the literature experimental data of *Durst et al.* [22] they found a reasonable agreement with experimental results for both the liquid and the gas phases.

In the present case study, we use the two-fluid model of *Mat et al.* [15] and *Jinsong et al.* [16] to numerical simulation of bubbly flow in a cylinder with axial steady-state injection of gas. Like *Jinsong et al.* [16] we use the same operating parameters as the experiments by *Durst et al.* [22]. Finally the predicted results are compared with the numerical results of *Jinsong et al.* [16]. Comparisons between the predictions and the numerical results illustrate that the predictions are in good agreement with the literature datas.

Numerical method

The governing equations are discreted via the finite volume technique and then are solved by the SIMPLE algorithm. In order to increase the accuracy of calculations, the power-law scheme is employed to approximate the convection-diffusion terms. Furthermore, grid sensitivity is examined to ensure sufficient spatial resolution. The results reported are based on the mesh of 50×100 uniform grids.

Results and Discussions of the case study

The predicted results include the gas distribution and velocity field for both the liquid and the gas phases. The predicted results have been compared with numerical data of *Jinsong et al.* [16] for both the gas and the liquid phases. Comparisons between the predictions and the numerical results of *Jinsong et al.* [16] illustrate that the predictions are in good agreement with the literature datas.

The simulated axial bubble velocity along the centerline of vessel (normalized by the maximum bubble axial velocity $w_{g,max}$) is shown in Fig. 3 where it is compared with the numerical results of *Jinsong et al.* [16]. Reasonable agreement is found between the predictions and the numerical results of *Jinsong et al.* [16]. Near the gas entrance, the bubbles are driven by the buoyancy force and move upwards. After a certain distance from the leading point, bubbles reach a terminal velocity and move up at this speed until they

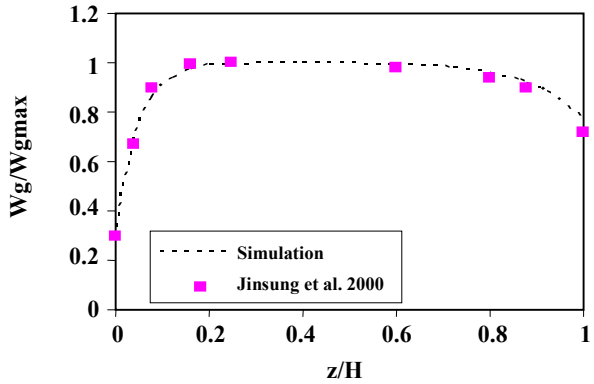

Fig. 3: Gas phase axial velocity along the centerline of vessel.

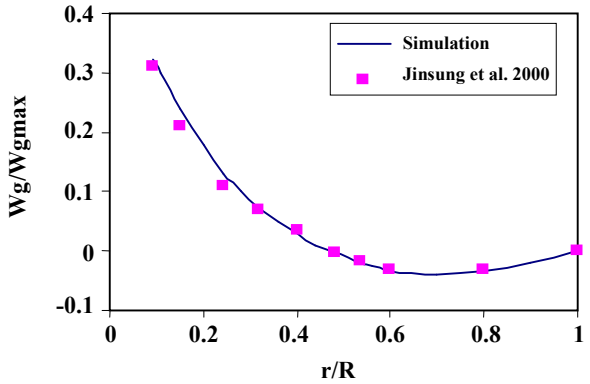

Fig. 4: Predicted vertical component of liquid velocity at the vertical section of z/H=0.36.

reach the vicinity of the free surface where the bubble velocities are reduced due to the increase of drag force caused by increasing relative motion between bubble and liquid phases. It should be noted that because of natural convection the liquid flow is a result of friction between two phases. Therefore, when the liquid approaches the free surface, the axial velocity decreases while the radial velocity increases. As a result, the liquid shifts in the radial direction and causes the liquid circulation in the container.

Fig. 4 shows the comparison between the simulated profiles of axial liquid velocity at the vertical section of (z/H=0.36) and the numerical results of *Jinsong et al.* [16]. Here, the maximum bubble velocity $w_{g,max}$, is used to normalize the liquid velocity. It is seen that the maximum liquid velocity is located on the centerline of the plume where the maximum gas volume fraction is formed. The significant decrease of axial liquid velocity along the lateral direction may be attributed to the decrease of bubble void fraction due to the weakness of bubble diffusion. Our simulation is in reasonable agreements with the numerical results of *Jinsong et al.* [16].

The predicted gas void fraction profiles at three vertical sections in the cylinder are presented in Figs. 5, 6 and 7. It is seen that the maximum gas volume fraction is located in the centre of the container. Most of the bubbles are located in the central region of the container, and bubble volume fraction near the gas injection orifice is higher than that being far away from the orifice. The significant decrease of gas void fraction along the lateral direction of cylinder may be attributed to the decrease of bubble diffusion.

Fig. 8 shows the Figs. 5, 6, 7 in a diagram. It should be noted that the gas volume fractions for r/R>0.2 is two orders of magnitude lower than the central regime and hence their value cannot be observed on a linear scale shown in Fig. 8. Similar results have been observed in the numerical work of *Jinsong et al.* [16].

RESULTS AND DISCUSSION

The primary motivation for this study was to establish the viability of a modified two-fluid model for predicting the detailed electrophysical phenomena involved in the electrolysis process membrane chlor-alkali cells. The predicted results include the chlorine gas distribution, velocity field and the effects of some processing parameters on the chlorine evolution. The predicted gas void fraction profiles at three vertical sections in the system (H is the height of the electrode) are presented in Fig. 9. In this figure and the subsequent figures x=0mm corresponds to the location of the electrode while x=4mm is the membrane location. The predicted void fraction being the highest near the electrode, drops sharply within about 1 mm and then decreases gradually towards the membrane. The lateral void fraction distribution also increases from the bottom to the top of the electrode, due to the mixing and diffusion of the gas phase along the channel. The significant decrease along the lateral direction may be attributed to the forced convection. Although the void fraction is significantly higher towards the top of the channel, the rate of gas release decreases in this direction mainly due to a decrease in the current density as the void fraction increases. Similar results have been observed in the numerical work of *Mat et al.* [15].

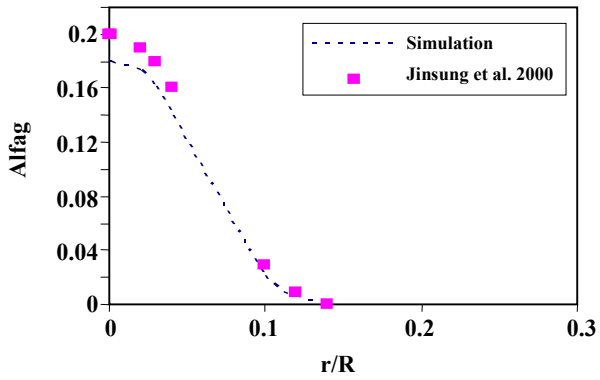

Fig. 5: Predicted gas void fraction distribution at the vertical section of z/H=0.06.

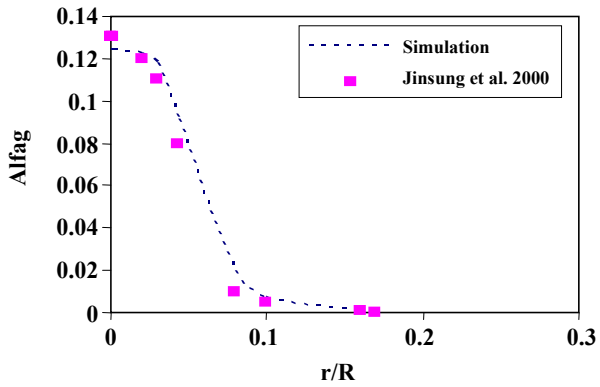

Fig. 6: Predicted gas void fraction distribution at the vertical section of z/H=0.36.

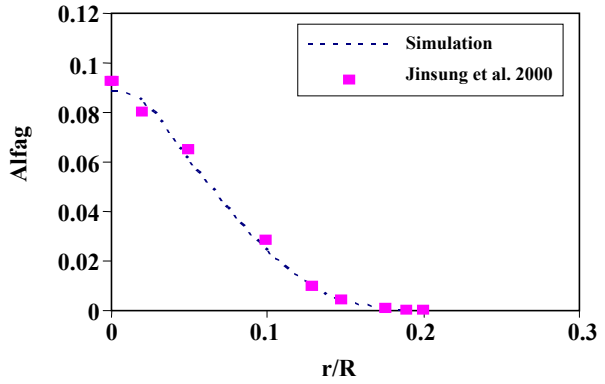

Fig. 7: Predicted gas void fraction distribution at the vertical section of z/H=0.9.

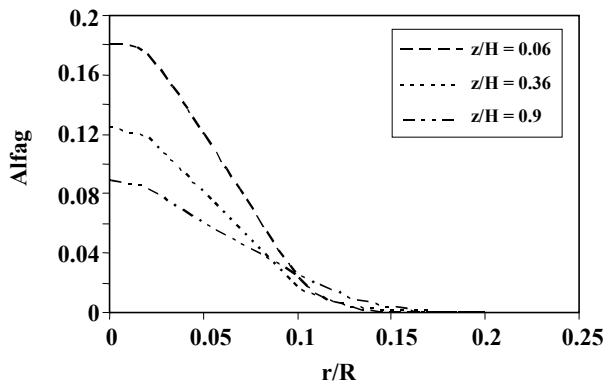

Fig. 8: Predicted gas void fraction distribution at three vertical sections of z/H=0.06,0.36,0.9.

The vertical velocities of the gas and the liquid phases at several locations in natural convection state are compared in Figs. 10 and 11. The dashed lines represent the gas phase while dashed points represent the liquid phase. It is seen that both velocities are higher at the vicinity of the electrode and become weaker through the center. This result may be associated with the presence of the gas phase. Since the density of the gas phase is much lower than the continuous phase, the buoyancy force generated due to the density difference which drives the flow, becomes the most effective near the electrode (where the void fraction is the largest). The gas phase velocity is higher than the liquid velocity along the cell. It should be noted that because of the natural convection, the liquid flow is a result of friction between two phases. At the vicinity of the free surface, there is a significant difference between velocities of both phases since the liquid particles change direction here, while the gas phase freely escapes from the free surface. The influence of gas phase becomes more significant towards the top of the electrode (y=3H/4) and the velocity across the cell increases. The observed increase in velocity away from the electrode may be explained by the increased shear and increased void fraction in the lateral direction.

The effect of the electrolyte flow rate on the gas evolution at the mid-section of the electrode (y=H/2), is presented in Fig. 12. It is seen that, gas release increases with an increase in the electrolyte velocity. This trend is due to the decrease in the residence time of the gas bubbles on the electrode, resulting in an enhanced electrochemical reaction. At higher velocity, the gas motion is confined to a small region in the vicinity of the electrode. Due to the strong electrolyte flow the gas bubbles cannot diffuse in the lateral direction. On the other hand, at a lower velocity, the gas release rate significantly decreases due to the increased residence time of bubbles that attenuates the electrochemical

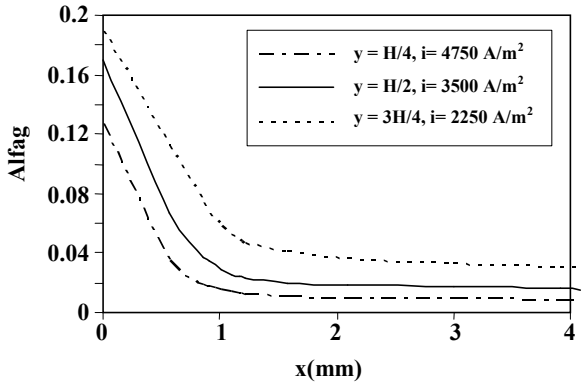

Fig. 9: Predicted gas void fraction distribution at three locations along the channel.

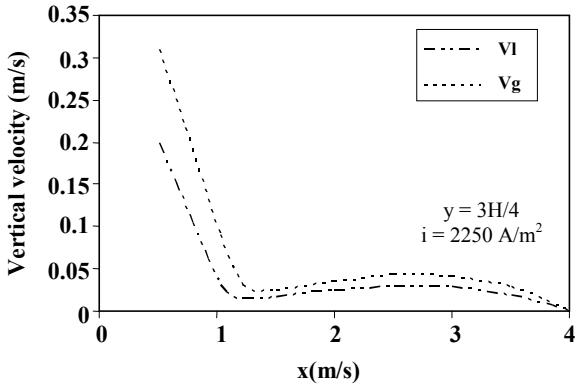

Fig. 11: Estimated vertical component of liquid and gas velocities (y=3H/4).

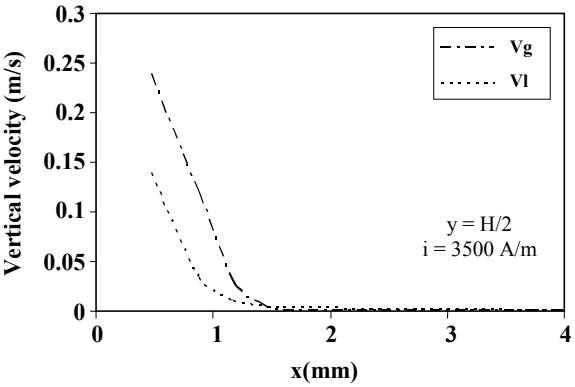

Fig. 10: Estimated vertical component of liquid and gas velocities (y=H/2).

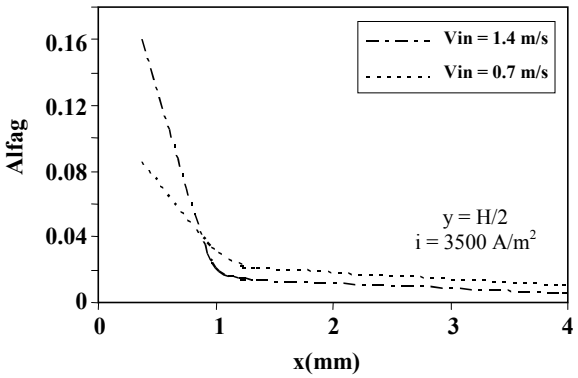

Fig. 12: Effect of the electrolyte flow rate on the gas release (y=H/2).

reaction. At an intermediate velocity level the gas bubbles can penetrate far into the electrolyte due to molecular diffusion and mixing.

The effect of the current density on the gas release at the mid-section of the electrode (y=H/2) is shown in Fig. 13. It is seen that the gas release rate increases at higher current densities as expected. At higher current densities gas penetrates at lateral direction mainly because of the increase in lateral gas velocities. It is seen that the chlorine release rate is not proportional to the increase in the current density. This is the result of accumulation of gas on the electrodes which adversely affects the chemical reaction rate. Since the inflow velocity of the electrolyte is kept constant, the lateral gas penetration is enhanced at higher current densities. Similar results have been observed in the experimental work of *Riegel et al.* [2].

The effect of the gap distance on the gas evolution at the lateral section of (x=1mm) is illustrated in Fig. 14 (L being the width of the channel). In this study, current density and inlet velocity of electrolyte are kept constant. It is seen that the void fraction decreases at the wider gap distances between the two electrodes. This may be attributed to the increased flow rate which swept formed gas easily at the larger gap distances. On the other hand, although void fraction decreases at a higher gap distance, the gas released in a time interval increases because of the higher flow rates.

CONCLUSIONS

A two-phase flow model has been used to predict the flow characteristics, chlorine gas release rate, and void distribution in a vertical membrane electro-chemical cell in both natural and forced convection states. This model involves the solution of transport equations for each phase with allowance to interphase mass and momentum transfer. In order to examine the validity of these model, numerical simulations of a

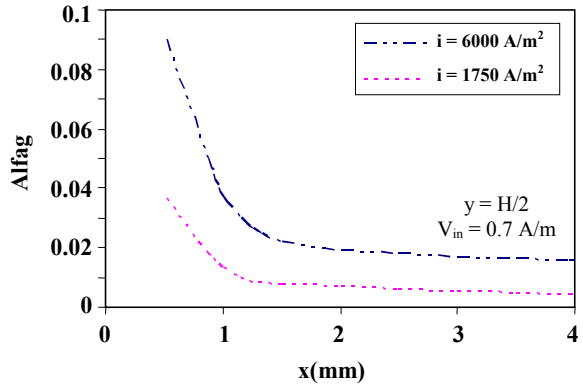

Fig. 13: Effect of current density on the gas release (vin=0.7 m/s).

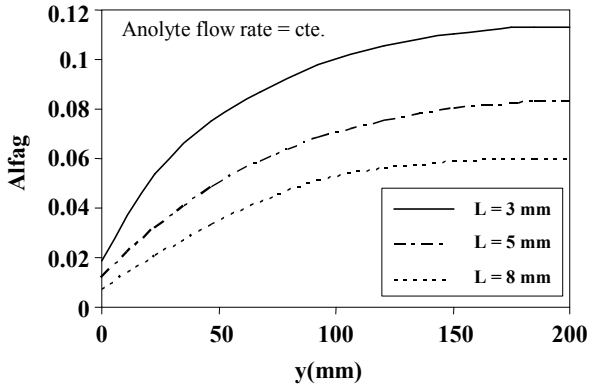

Fig. 14: Estimated gas void fraction distribution on the anode at different cell gap distance along the electrode (x=1 mm).

bubble-driven flow caused by the bottom injection of gas into a liquid bath has been conducted. Comparisons between the predictions and the literature numerical datas of *Jinsong et al.* [16] illustrate that the present model is capable of capturing a reasonable agreement with numerical results for both the liquid and gas phases.

In natural convection state, the main characteristic of the system is a buoyancy generated flow due to the large density difference between liquid and gaseous phases. The predicted void fraction increases along both the vertical and horizontal directions. The vertical increase is attributed to the accumulation of gas towards the top of the cell due to buoyancy, while the lateral increase is a result of the molecular diffusion. It is found that both velocities of gas and liquid are higher at the vicinity of the electrodes and become weaker through the center. This result may be associated with the presence of the gas phase.

Since the density of the gas phase is much lower than the continuous phase, the buoyancy force generated due to the density difference driving the flow, becomes the most effective near the electrode (where the void fraction is the largest). The gas release rate increases as the electrolyte flow velocity increases due to the consequent decrease in the residence time of bubbles on the electrode. The gas release rate was enhanced with higher applied current density; however, the increase is found to be not linear with the increase in current density due to the higher bubble content on the electrode surface diminishing the penetration of fresh electrolyte to reaction sites; thus, reducing the gas release rate. Therefore, for an efficient electrolysis process gas released should be removed from the reaction sites to increase surface areas available for the reaction.

This work represents a major advancement in the study of the electrolytic production of the chlorine. Numerical Simulation of turbulent two-phase flow regime, considering the effect of ion transfer, will be the subject of a future study.

Nomenclatures

C_d	Drag coefficient
D	Diffusion coefficient (m^2/s)
d_b	Bubble diameter (m)
F	Faraday constant (C/mol)
F_r	Volumetric inter-fluid friction (kg/m^2s)
i	Current density (A/m^2)
P	Static pressure (pa)
R	Universal gas constant (J/mol.K)
Re	Reynolds number
T	Temperature (K)
u	X-velocity vector (m/s)
V	y&r-velocity vector (m/s)
W	Z-velocity vector (m/s)
F_b	Buoyancy forces (kg/m^2s^2)
G	Gravity vector (m/s^2)
H	Height of electrode & cylinder (m)
W	Width of channel (m)
R	Radius of cylinder (m)

Greek letters

α	Void fraction
ρ	Density (kg/m^3)
η	Anodic over potential, (Volt)

ϕ	Electric potential, (Volt)
μ	Viscosity (N.s/m^2)

Subscripts

b	Bubble
g	Gas phase
l	Liquid phase
nb	Beighbor
eff	Effective
P	Unknown node
W	West of node P
E	East of node P
N	North of node P
S	South of node P

Acknowledgements

The authors would like to thank the petrochemical R&D Company and Amirkabir University of Technology for supporting this study.

Received : 28th May 2007 ; Accepted : 2nd September 2007

REFERENCES

[1] Vogt, H., *New York Plenum Press*, **6**, 445, (1983).
[2] Reigel, H., Mitrovic, J., Stephan, K., *Appl. Electrochem.*, **28**, 10, (1998).
[3] Fukunaka, Y., Kondo, Y., *Metall Rev. MMIJ1*, **5**, 9, (1988).
[4] Boissonneau, P., Byrne, P., *Appl. Electrochem.*, **30**, 767, (2000).
[5] Hine, F., Murakami, K., *Electrochem. Soc.*, **127**, 292, (1980).
[6] Nagai, N., Takeuchi, M., Kimura, T., Oka, T., *Hydrogen Energy*, **28**, 35, (2003).
[7] Byrne, P., Simonsson D., Fontes, E., Lucor, D., Marty, P., Thibault, J.P., The Netherlands Kluwer Academic Publishers, **137**, (1999).
[8] Ozil, P., Aurousseau, M., Mitu, S., Marty, P., Thibault, J.P., The Netherlands Kluwer Academic Publishers, **153**, (1999).
[9] Lockart, R.W., Martinelli, R.C., *Chem. Eng. Prog.*, **45**, 39, (1949).
[10] Heal, G.R., Kuhn, A.T., Lartey, R.B., *Electrochem. Soc.*, **124**, 1960, (1977).
[11] Janssen, L.J.J., Hoogland, J.G., *Electrochim. Acta*, **15**, 1013, (1970).
[12] Boxall, C., Kelsall, G. H., *I. Chem. E Symp. Ser*., **127**, 59, (1992).
[13] Dahlkild, A.A., *Fluid Mechanics*, **428**, 249, (2001).
[14] Celik, I., Wang, Y.Z., *Multiphase Flow,* **20**, 1053, (1994).
[15] Mahmut D. Mat, Kemal Aldas, Olusegun J. Ilegbusi, *Hydrogen Energy*, **29**, 1015, (2004).
[16] Jinsong Hua, Chi-Hwa Wang, *Chemical Engineering Scince*, **55**, 4159, (2000).
[17] Jean St. Pierre, Anthony A. Wragg, *Electrochemical Acta*, **38**, 1705, (1993).
[18] Mahmut D. Mat., Kemal Aldas, *Hydrogen Energy*, **30**, 411, (2005).
[19] Kemal Aldas, *Applied Mathematics and Computation*, **154**, 507, (2004).
[20] Clift, R., Grace, J.R., Weber, M.E., *Academic Press*, (1978).
[21] Vetter, K. J., *Academic Press Inc*., (1967).
[22] Durst, F., Taylor, A. M. K. P., Whitelaw, J. H., *Multiphase Flow*, **10**, 557, (1984).
[23] Durst, F., Schonung, B., Selanger, K., Winter, M., *Fluid Mechanics*, **170**, 53, (1986).
[24] Celik, I., Wang, Y. Z., Multiphase *Flow*, **20**, 1053, (1994).
[25] Johansen, S. T., Robertson, D. G. C., Woje, K., Engh, T. A., *Experiments*, **19B**, 745, (1988).
[26] Johansen, S. T., Boysan, F., *Mathematical Modelling*, **19B**, 755, (1988).
[27] Castillejos, A. H., Brimacombe, J. K., *Metallurgical Transactions*, **18B**, 659, (1987).